iScience, Volume *24*

Supplemental information

Human colorectal cancer-on-chip model to study the microenvironmental influence on early metastatic spread

Carly Strelez, Sujatha Chilakala, Kimya Ghaffarian, Roy Lau, Erin Spiller, Nolan Ung, Danielle Hixon, Ah Young Yoon, Ren X. Sun, Heinz-Josef Lenz, Jonathan E. Katz, and Shannon M. Mumenthaler

Table S2. Differential metabolites between D0 and D6 of endothelial channel effluent for the HCT116-CRC-on-Chip, Related to Figure 2.

Database source/Library	Metabolite Presumptive ID	Observed Molecular Weight	Fold Change	p value
IROA	5-Phospho-D-Ribose 1-Diphosphate	435.9554	5.07	2.58E-02
IROA	3-(4-Hydroxyphenyl)Lactate	182.0583	3.33	2.84E-02
IROA	Alpha-Ketoglutaric Acid	146.0216	3.21	2.79E-02
IROA	Citramalate	148.0374	2.68	9.39E-06
IROA	O-Acetyl-l-Serine	193.0535	2.98	2.73E-02
IROA	Itaconate	130.0264	2.94	2.57E-02
IROA	Tryptophan	204.0874	2.58	1.73E-02
IROA	Pyruvate	88.0158	-3.26	3.89E-03
IROA	Homocystine	314.0578	-3.26	4.58E-05
IROA	1-Hydroxy-2-Naphthoate	188.0476	-2.28	1.54E-02
IROA	Methyl Acetoacetate	116.0468	-4.39	1.13E-02
IROA	3-(2-Hydroxyphenyl)Propanoate	212.0648	-3.49	2.97E-02
IROA	Normetanephrine	243.1021	-3.54	1.23E-02
IROA	Dehydroascorbate	174.0173	-3.63	2.77E-02
IROA	Malate	133.0377	-2.16	3.81E-02
IROA	2,6-Dihydroxypyridine	155.9546	-2.52	3.35E-05
IROA	Lactate	90.0309	2.01	3.08E-02
IROA	Proline	115.0634	-2.01	1.21E-02
IROA	N-Acetyl-dl-Glutamic Acid	189.1651	-2.63	3.67E-02
IROA	N-Acetyl-l-Aspartic Acid	175.1396	-4.62	2.87E-02
IROA	Inosine	268.0808	2.39	1.27E-02
IROA	Ferulate	194.1806	-9,680	3.50E-03
IROA	Butanal	132.0769	-2.19	3.52E-02
IROA	Sarcosine	89.0477	-2.06	4.66E-03
IROA	Uridine-5-Monophosphate	324.1821	-31	2.20E-03
METLIN	(+)-Chebulic acid	402.0418	-2.67	4.77E-02
METLIN	2,7-Anhydro-alpha-N-acetylneuraminic acid	291.0952	-3.45	1.76E-03
METLIN	2-Aminoadenosine	282.1084	-2.85	8.90E-04
METLIN	3'-Amino-3'-deoxy-AMP	392.0786	-4.61	3.98E-02
METLIN	3'-O-Methyl-(-)-epicatechin-7-O-sulphate	414.0609	-3.63	2.33E-02
METLIN	5'-Methoxybilobetin	642.1323	-2.73	1.97E-02
METLIN	8-Hydroxy-3-chlorodibenzofuran	218.0109	3.35	3.26E-02
METLIN	AVE-1625	556.0857	-2.79	1.90E-02

Molecular Formula	C19 H42 N2 O22	650.2241	3.49	1.75E-02
Molecular Formula	C22 H21 N3 O21	663.0698	-4.71	2.40E-05
Molecular Formula	C24 H21 N6 O22	745.0721	-2.75	4.43E-05
Molecular Formula	C26 H21 N9 O23	827.0735	-2.73	2.02E-05
Molecular Formula	C28 H29 O15	605.1506	-2.2	4.18E-02
Molecular Formula	C4 H2 N O3 S2	175.9456	2.39	2.34E-02
Molecular Formula	C40 H17 N10 O17	909.0706	-3.64	2.46E-04
Molecular Formula	C5 H4 N2	92.0362	-2.07	1.07E-02
METLIN	Dihydropteroic acid	360.1175	-2.78	3.08E-02
METLIN	Distemonanthin	404.0397	-2.7	4.19E-02
METLIN	fumarylacetic acid	158.0212	2.82	3.71E-02
METLIN	Galactosylglycerol	314.1227	2.07	8.27E-03
METLIN	Hydrouracil (Dihydrothymine)	128.0589	2.34	4.33E-03
METLIN	N-Nitrosodiethylamine	102.0796	2.3	7.07E-03
METLIN	Phosphophosphinate	335.0578	-2.19	1.71E-04

Table S3. Differential metabolites between D0 and D6 of epithelial channel effluent for the HT29-CRC-on-Chip, Related to Figure 2.

Database source/Library	Metabolite Presumptive ID	Observed Molecular Weight	Fold Change	p value
IROA	1-Methyladenosine	281.1137	-12	1.14E-02
IROA	3-Ureidopropionate	132.0533	-2.91	7.45E-08
IROA	5'-Methylthioadenosine	314.1091	2.18	5.28E-03
IROA	Raffinose	564.172	3.52	2.24E-03
IROA	Aspartate	133.0373	3.31	2.96E-03
IROA	Ornithine	132.0895	-2.43	9.24E-07
IROA	Flavin Adenine Dinucleotide	785.1841	2.41	1.23E-03
IROA	Inosine	268.0791	2.78	3.59E-03
IROA	L-Proline	115.0629	-2.80	2.25E-09
IROA	N-Acetylneuraminate	326.1354	6.45	8.41E-04
IROA	Pyrrole-2-Carboxylate	133.011	-3.52	2.44E-12
IROA	Sarcosine	89.0471	-3.31	3.72E-10
IROA	Sucrose	342.1176	-2.60	1.03E-03
IROA	Xanthine	152.0325	-3.80	5.62E-06
IROA	Citrate	192.0271	-2.17	2.61E-04
IROA	5-Oxo-l-proline	129.0431	-2.70	1.57E-04
IROA	Lactate	90.0312	-2.4	5.09E-03
IROA	Ferulate	194.0573	-6.16	1.04E-03

IROA	1-Methyl-6,7-Dihydroxy-1,2,3,4-Tetrahydroisoquinoline	179.0941	-3.75	3.28E-02
IROA	L-Kynurenine	208.084	-23	1.54E-02
IROA	Cholesteryl Acetate	428.365	2.28	4.50E-02
IROA	2-Hydroxybutyric Acid	126.0315	-53	9.31E-04
METLIN	1,2-Dihydroxynaphthalene-6-sulfonate	286.0166	3.11	2.00E-03
METLIN	2-(beta-D-Glucosyl)-sn-glycerol	300.103	-3.1	7.82E-04
METLIN	2-C-Methyl-D-erythritol 2,4-cyclodiphosphate	323.9953	-2.2	4.32E-04
METLIN	2-Phenylaminoadenosine	358.1384	-4.1	3.73E-05
METLIN	3-Hydroxy-L-tyrosyl-AMP	526.1335	2.51	1.57E-04
METLIN	3-Hydroxy-OPC4-CoA	1003.2531	2.76	7.31E-04
METLIN	6''-(4-Carboxy-3-hydroxy-3-methylbutanoyl)hyperin	608.1362	2.31	1.66E-04
METLIN	6-Mercaptopurine ribonucleoside 5'-diphosphate	461.0225	-3.2	3.86E-11
METLIN	AM679	417.0581	-3	1.54E-09
METLIN	Azamethiphos	345.9607	2.16	2.50E-02
METLIN	Butoconazole	456.0233	3.93	5.22E-03
Molecular Formula	C13 H6 N O7	288.0157	3.01	2.41E-03
Molecular Formula	C16 H11 N6 O16	543.0254	-3.4	6.42E-11
Molecular Formula	C20 H13 N6 O18	625.0279	-3.2	4.80E-11
Molecular Formula	C21 H15 N10 O16	663.065	-3.6	2.88E-08
Molecular Formula	C21 H35 N8 O17 S	703.1831	2.62	2.37E-03
Molecular Formula	C22 H17 N6 O20	685.0471	-3.3	2.54E-11
Molecular Formula	C25 H15 N11 O18 S	789.0297	-2.6	2.82E-10
Molecular Formula	C25 H32 N4 O24	772.1405	2.05	2.04E-04
Molecular Formula	C27 H17 N19 O	623.1863	2.63	9.35E-04
Molecular Formula	C27 H24 N18 O11	776.1849	3.1	1.96E-04
Molecular Formula	C29 H29 N22 O4 S2	813.2188	2.72	1.10E-03
Molecular Formula	C33 H54 N O26 S2	944.2348	4.5	3.85E-04
Molecular Formula	C34 H13 N13 O14	827.0675	-2.6	3.79E-08
Molecular Formula	C34 H13 N14 O21	953.0244	-2.3	6.97E-09
Molecular Formula	C34 H15 N8 O21	871.0308	-2.4	1.82E-09
Molecular Formula	C35 H11 N11 O10	745.0668	-3.4	4.98E-08
Molecular Formula	C42 H19 N13	705.187	2.34	9.18E-04
METLIN	Cyanidin 3-O-[b-D-Xylopyranosyl-(1-2)-[(4-hydroxybenzoyl)-(-6)-b-D-glucopyranosyl-(1-6)]-b-D-galactopyranoside]	862.2344	4.4	2.04E-04
METLIN	Eujambolin	542.1054	2.39	3.05E-03

METLIN	Floxacillin	499.0614	-3.1	1.53E-08
METLIN	Flupyrsulfuron-methyl	465.0653	-2.1	4.78E-09
METLIN	Gossypetin 3-sophoroside-8-glucoside	821.206	3.78	2.22E-03
METLIN	His Phe Gly	381.1381	34.1	2.05E-03
METLIN	Isoscutellarein 7-(6'''-acetylallosyl-(1-2)-6''-acetylglucoside)	694.1832	3.22	2.54E-04
METLIN	Leucodelphinidin 3-[galactosyl-(1-4)-glucoside]	646.1742	3.13	6.06E-03
METLIN	Leu-Nap-OH	482.1693	3.59	3.80E-03
METLIN	L-Rhamnulose 1-phosphate	304.0556	4.83	4.93E-03
METLIN	N-(4-hydroxyphenyl)ethoxycarbothioamide	197.0535	-2.6	2.90E-06
METLIN	N-benzyl-1-methyl-1H-pyrazolo[3,4-d]pyrimidin-4-amine	239.117	-2	2.23E-02
METLIN	N-Cyclohexylformamide	127.1005	-1100	4.94E-07
METLIN	Obtusol	472.0021	2.6	1.78E-03
METLIN	Perfluidone	379.0197	-3	2.66E-12
METLIN	Phosphophosphinate	297.0171	-3.8	1.80E-10
METLIN	Photinus luciferin	325.9949	-2.3	2.47E-04
METLIN	Primflaside	728.1765	3	5.92E-04
METLIN	PtdIns-(4,5)-P2 (1,2-dihexanoyl)	690.1374	2.2	1.67E-04
METLIN	Pyridoxamine-5'-Phosphate	294.0578	-180	1.90E-04
METLIN	Tamarixetin 3-O-sulfate	396.0145	3.51	1.85E-03
METLIN	Thioridazine 2,5-disulfoxide	419.1748	-2.7	3.87E-05
METLIN	UDP-L-Ara4N	581.0635	-3.5	7.06E-09
METLIN	PC(O-12:0/2:0)	467.3018	15	4.22E-02
METLIN	L-Arogenate	227.0789	-13	4.47E-02
METLIN	PS(P-16:0/15:1(9Z))	703.4809	2.32	4.54E-02
METLIN	Glu Tyr	310.1154	-3.22	3.88E-02

Table S4. Differential metabolites between D0 and D6 of endothelial channel effluent for the HT29-CRC-on-Chip, Related to Figure 2.

Database source/Library	Metabolite Presumptive ID	Observed Molecular Weight	Fold Change	p value
IROA	N-Acetylneuraminate	326.1354	2.64	2.79E-03
IROA	Sucrose	342.1176	-53	2.02E-03
IROA	Hypoxanthine	136.038	3.62	1.60E-03
IROA	2-Hydroxybutyric Acid	126.0315	-2.31	2.44E-02
IROA	Inosine	268.0791	2.26	2.00E-03

METLIN	His Phe Gly	381.1381	2.15	3.74E-03
METLIN	N-benzyl-1-methyl-1H-pyrazolo[3,4-d]pyrimidin-4-amine	239.117	-4.1	1.06E-04
METLIN	N-Cyclohexylformamide	127.1005	-14	5.96E-03
METLIN	3,4-Dihydroxyphenylglycol O-sulfate	250.0127	-2	4.50E-02
METLIN	Thr Thr Glu	366.1749	-53	3.86E-02
METLIN	L-Rhamnulose 1-phosphate	304.0556	2.2	1.90E-03
METLIN	Suprofen	306.054	2.07	1.71E-03
METLIN	2-Phenylaminoadenosine	358.1384	-17	2.11E-03
METLIN	Nicarbazin	302.0626	-5.76	4.20E-03
METLIN	2-Hexaprenyl-6-methoxy-1,4-benzoquinol	565.447	21	3.66E-02
METLIN	His Ala Ser	313.138	6.99	4.62E-02
Molecular Formula	C25 H8 N8 O18	707.9943	67	2.98E-02

Table S6. Top significantly altered metabolic pathways from IPA analysis of differential metabolites between Intestine Chip and HCT116-CRC-on-Chip epithelial effluent on D6, Related to Figure 2.

Metabolic Pathway	p value	Metabolites
Alanine Metabolism	3.04E-04	2-oxoglutaric acid, L-alanine, L-glutamic acid, pyruvic acid
TCA Cycle II (Eukaryotic)	2.95E-04	2-oxoglutaric acid, citric acid, fumaric acid, L-malic acid, oxalacetic acid, succinic acid
Purine Nucleotides Metabolism	8.84E-03	adenosine, guanine, guanosine, hypoxanthine, inosine, uric acid, xanthine, xanthosine
Adenosine Nucleotides Metabolism	2.15E-05	adenosine, hypoxanthine, inosine, uric acid, xanthine
Glutamate Metabolism	2.12E-04	2-oxoglutaric acid, fumaric acid, L-glutamic acid, oxalacetic acid
Superpathway of Methionine Degradation	8.42E-04	2-oxoglutaric acid, adenosine, L-cysteine, L-glutamic acid, L-homocysteine, L-methionine, pyruvic acid

Table S7. Top significantly altered metabolic pathways from IPA analysis of differential metabolites between Intestine Chip and HCT116-CRC-on-Chip endothelial effluent on D6, Related to Figure 3.

Metabolic Pathway	p value	Metabolites
Glycine Betaine Degradation	1.06E-04	L-homocysteine, pyruvic acid, sarcosine
Alanine Metabolism	3.42E-04	2-oxoglutaric acid, pyruvic acid
H1F1 α signaling	8.47E-04	lactic acid, pyruvic acid
Adenine and Adenosine Salvage pathway	2.60E-04	inosine, phosphoribosyl pyrophosphate

Table S8. Analysis of over-expressed cytokines secreted by patient-derived CAFs (Z-score > 0.5), Related to Figure 5 and Figure S7.

000UE	000US	000U8	000W8	Cytokines	Count
TRUE	TRUE	TRUE	TRUE		0
FALSE	TRUE	TRUE	TRUE		0
TRUE	FALSE	TRUE	TRUE		0
FALSE	FALSE	TRUE	TRUE	IL-17A; LIF; Lipocalin-2	3
TRUE	TRUE	FALSE	TRUE		0
FALSE	TRUE	FALSE	TRUE	ENA-78; GRO-alpha; MCP-1	3
TRUE	FALSE	FALSE	TRUE	C-Reactive_Protein; FGF-7; FGF_basic; IL-11; Myeloperoxidase; TNF-alpha	6
FALSE	FALSE	FALSE	TRUE	Angiogenin; ICAM-1; IL-4; IL-12_p70; IL-6; IL-8; IL-10; IL-23; IL-24; RANTES; PDGF-AA; PDGF-AB/BB; VEGF; TARC; TFF3; VCAM-1; TIM-3	17
TRUE	TRUE	TRUE	FALSE		0
FALSE	TRUE	TRUE	FALSE	DPPIV; Flt-3_Ligand; IL-18_BPa; MIG	4
TRUE	FALSE	TRUE	FALSE	FGF-19; Thrombospondin-1; Vitamin_D_BP	3

FALSE	FALSE	TRUE	FALSE	Angiopoietin-2; BDNF; Complement_Component_C5/C5a; CD14; CD30; Adiponectin; Cripto-1; EMMPRIN; CD40_ligand; G-CSF; GDF-15; GM-CSF; Fas_Ligand; IL-1beta; IL-1ra; IL-2; IL-3; Growth_Hormone; HGF; IL-13; IL-15; IL-16; IL-19; IL-34; IL-22; Leptin; MIP-3beta; RBP-4; Resistin; Osteopontin; ST2; CD31	32
TRUE	TRUE	FALSE	FALSE	Cystatin_C; IGFBP-2; IFN-gamma; IL-31; IL-32; MIP-1alpha/MIP-1beta	6
FALSE	TRUE	FALSE	FALSE	BAFF; Angiopoietin-1; EGF; IGFBP-3; IL-1alpha; IL-5; IL-33; IP-10; I-TAC; Kallikrein_3; IL-27;M-CSF; MIP-3alpha; MMP-9; MCP-3; TfR	16
TRUE	FALSE	FALSE	FALSE	Apolipoprotein_A-I; Dkk-1; Chitinase_3 like_1; Complement_Factor_D; Endoglin; MIF; PF4; RAGE; Relaxin-2; SDF-1alpha; Pentraxin-3; TGF-alpha; uPAR; SHBG	14

Table S9. Analysis of under-expressed cytokines secreted by patient-derived CAFs (Z-score < 0.5), Related to Figure 5 and Figure S7.

000UE	000US	000U8	000W8	Cytokines	Count
TRUE	TRUE	TRUE	TRUE		0
FALSE	TRUE	TRUE	TRUE		0
TRUE	FALSE	TRUE	TRUE		0
FALSE	FALSE	TRUE	TRUE	IGFBP-3; IL-31; IL-32; I-TAC; M-CSF; MCP-3; SDF-1alpha	7
TRUE	TRUE	FALSE	TRUE		0
FALSE	TRUE	FALSE	TRUE	Apolipoprotein_A-I; Dkk-1; FGF-19; Fas_Ligand; IL-1beta; Osteopontin; Pentraxin-3; Thrombospondin-1; Vitamin_D_BP	9
TRUE	FALSE	FALSE	TRUE	DPPIV; Flt-3_Ligand; G-CSF; GDF-15; IL-18_BPa	5
FALSE	FALSE	FALSE	TRUE	Angiopoietin-2; BAFF; BDNF; Complement_Component_C5/C5a; EGF; EMMPRIN; CD40_ligand; Chitinase_3-like_1;	24

				Complement_Factor_D; IL-1alpha; IL-1ra; IFN-gamma; IL-16; IL-5; IL-33; Kallikrein_3; MIG; MIP-1alpha/MIP-1beta; MIP-3alpha; MIP-3beta; MMP-9; PF4; RAGE; Relaxin-2	
TRUE	TRUE	TRUE	FALSE		0
FALSE	TRUE	TRUE	FALSE	Angiogenin; FGF_basic; IL-6; IL-10; Myeloperoxidase; uPAR; SHBG; TFF3	8
TRUE	FALSE	TRUE	FALSE	ENA-78; GRO-alpha; TARC	3
FALSE	FALSE	TRUE	FALSE	Cystatin_C; C-Reactive_Protein; Endoglin; IGFBP-2; IL-11; IL-12_p70; IL-27; MIF; MCP-1; Serpin_E1; TfR; TGF-alpha; VCAM-1; TIM-3	14
TRUE	TRUE	FALSE	FALSE	CD14; CD30; Adiponectin; GM-CSF; IL-2; IL-3; Growth_Hormone; ICAM-1; IL-4; IL-15; IL-17A; IL-8; IL-19; Leptin; LIF; Lipocalin-2; Resistin; PDGF-AB/BB; CD31	19
FALSE	TRUE	FALSE	FALSE	Cripto-1; FGF-7; IL-22; IL-23; RANTES; RBP-4; PDGF-AA; TNF-alpha; VEGF; ST2	10
TRUE	FALSE	FALSE	FALSE	Angiopoietin-1; HGF; IL-13; IL-34; IP-10; IL-24	6

Table S10. Clinical details of patient samples, Related to Figures 3 and 5 and STAR Methods.

Cell Model	Sample ID	Sex	CRC Stage	Resection Site	Molecular Information of Patient Tumor	Clinical Treatment
Organoid	000US	Male	IIb	Colon	KDR, KRAS, TP53, SMAD4 mutant	Adjuvant Xeloda
CAF	000U8	Female	I	Colon	Microsatellite stable (MSS)	Unknown
CAF	000US	Male	IIb	Colon	KDR, KRAS, TP53, SMAD4 mutant	Adjuvant Xeloda
CAF	000UE	Female	IIIB	Colon	MSS	Adjuvant FOLFOX
CAF	000W8	Male	IVa	Liver	CHEK2 T367M, MSS	Adjuvant Xeloda, switched to FOLFOX

Table S11. Gene specific primers for qPCR, Related to Figures 4 and 5 and STAR Methods.

Gene	Direction	Sequence 5' → 3'
Human GAPDH	Forward	TCTGGTAAAGTGGATATTGTTG
	Reverse	GATGGTGATGGGATTTCC
Human E-Cadherin	Forward	TTTGTACAGATGGGGTCTTGC
	Reverse	CAAGCCCACTTTTCATAGTTCC
Human EpCam	Forward	AATGTGTGTGCGTGGGA
	Reverse	TTCAAGATTGGTAAAGCCAGT
Human αSMA	Forward	CAATGGCTCTGGGCTCTGTAAG
	Reverse	TGTTCTATCGGGTACTTCAGGGTC
Human Fibronectin	Forward	TCCCTCGGAACATCAGAAAC
	Reverse	CAGTGGGAGACCTCGAGAAG
Human Vimentin	Forward	GAGAACTTTGCCGTTGAAGC
	Reverse	GCTTCCTGTAGGTGGCAATC

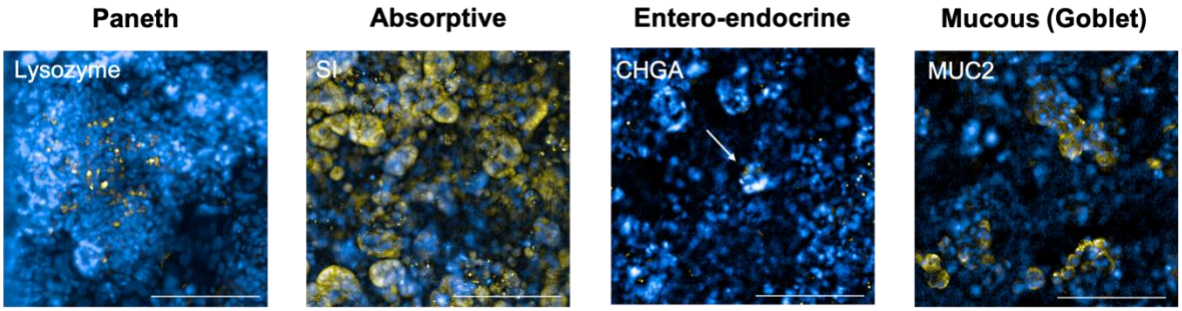

Figure S1. Caco2 Intestine Chip exhibits different cell types present in the human intestine, Related to Figure 1. Representative confocal immunofluorescent images of Caco2 C2BBe1 cells on day 6 in the top epithelial channel of the Intestine Chip stained for markers of Paneth cells (Lysozyme), absorptive cells (Sucrose Isomerase; SI), entero-endocrine cells (Chromogranin A; CHGA) and mucus-secreting Goblet cells (Mucin 2; MUC2). Cell nuclei are labeled with DAPI (blue). Scale bars represent 200 µm.

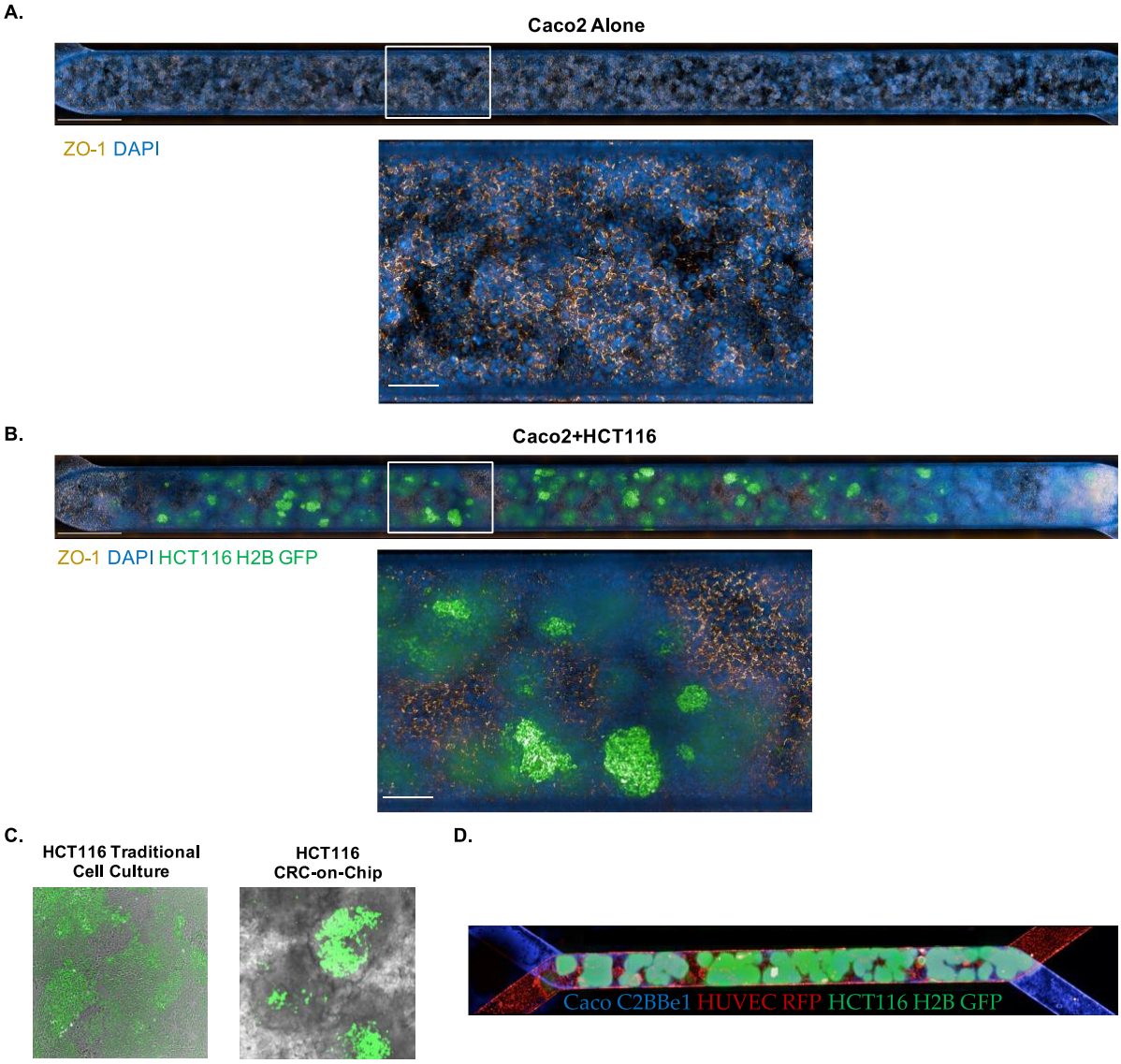

Figure S2. Tight junction formation and tumor cell morphology in the HCT116-CRC-on-Chip, Related to Figure 1. A. Tiled maximum projection (60 µm Z-height) and zoomed-in (white box) confocal fluorescent images of the epithelial channel of the Caco2 Intestine Chip on day 6 stained for tight junction protein ZO-1 (gold). Cell nuclei are labeled with DAPI (blue). Scale bar represents 1 mm on the tiled image and 200 µm on the zoomed-in image. **B.** Tiled maximum projection (60 µm Z-height) and zoomed-in (white box) confocal fluorescent images of the epithelial channel of the HCT116-CRC-on-Chip on day 6 stained for tight junction protein ZO-1 (gold). HCT116 are labeled with H2B GFP (green) and cell nuclei are labeled with DAPI (blue). Scale bar represents 1 mm on the tiled image and 200 µm on the zoomed-in image. **C.** HCT116 H2B-GFP morphology was compared between traditional 2D cell culture and on-chip. **D.** Tiled confocal fluorescent image of the entire CRC Chip. HCT116 tumor cells are H2B GFP labeled, and HUVEC cells are RFP labeled. The nuclei of the top epithelial channel were stained with DAPI.

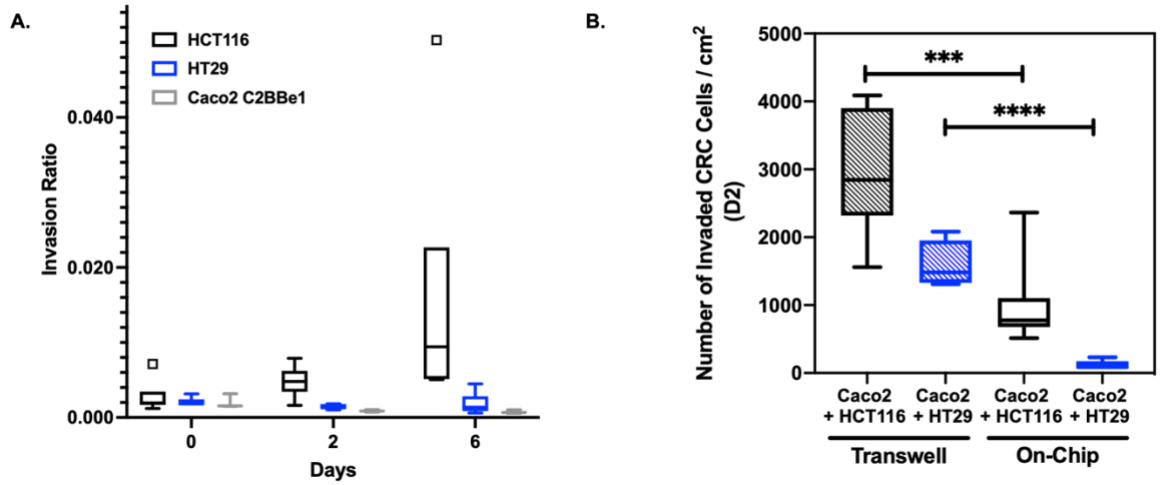

Figure S3. Validation of CRC-on-chip intravasation assay, Related to Figure 3. (A) Tumor cell (HCT116 or HT29) invasion was monitored over time by imaging the same chip regions at various timepoints, days 0, 2, 6, as described in Figure 3. Caco2 C2BBe1 cells were stained with Cell Tracker Green (CTG) and invasion of the Caco2 cells was measured in the Intestine Chip (N=3 Chips) on days 0, 2, and 6 as described in Figure 3. Raw invasion ratios were plotted as boxplots with Tukey's rule indicating an outlier (black box). In order to account for outliers, all data was normalized back to D0 invasion ratios as shown in Figure 3D. **(B)** Tumor cell invasion on-chip (day 2) was compared to traditional transwell invasion assays. HUVEC cells were seeded onto the bottom of the transwell membrane and tumor cells were seeded on the top of an ECM coated fluoroblok transwell and the GFP+ cells were counted 48 hours later on the bottom of the membrane. (N=6 Chips). Data are represented as boxplots and analyzed using an unpaired t-test; ***p<0.001; ****p<0.0001.

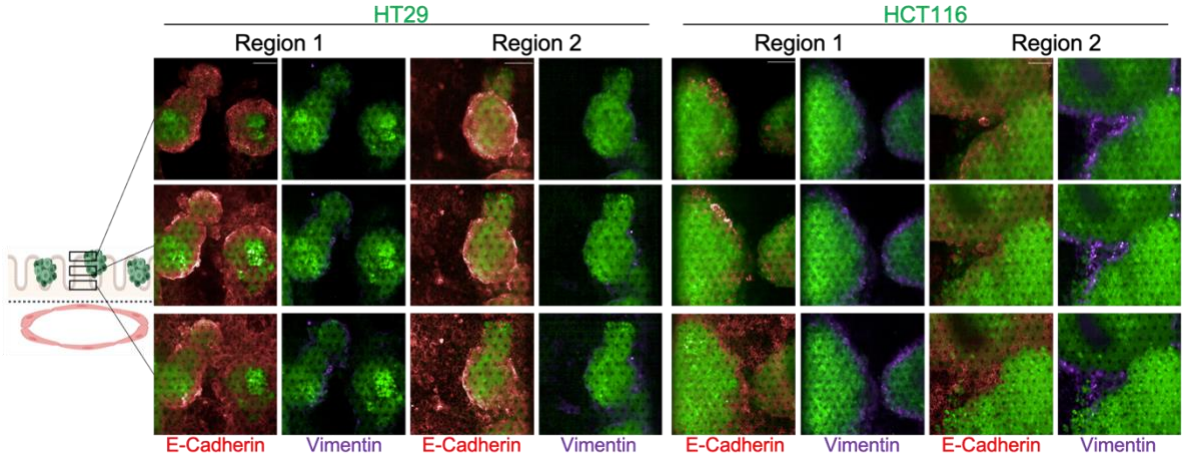

Figure S4. HT29 and HCT116 cells show different expression of epithelial and mesenchymal markers, Related to Figure 4. Representative images of HT29 and HCT116 clusters in top channel stained with E-cadherin and vimentin. Strong vimentin positive staining is observed on the periphery of HCT116 cell clusters compared to HT29 cells on day 10. Scale bars represent 100 µm.

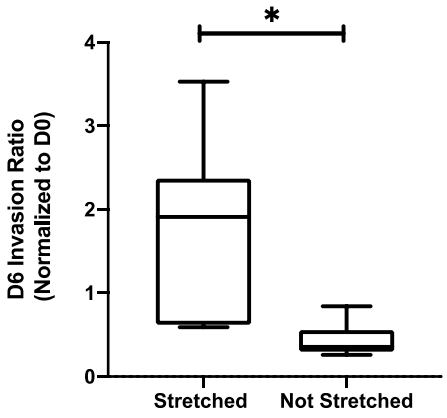

Figure S5. Peristalsis increases invasion in the CRC-on-Chips with HT29 tumor cells, Related to Figure 5. The invasion of HT29 H2B GFP cells was measured in the CRC-on-Chip (N=6 Chips) on day 6 of the experiment. Six regions of the chip were imaged via confocal microscopy and input into 3D reconstruction software for GFP+ cell quantification. An invasion ratio was calculated based on the number of GFP+ cells in the bottom channel compared to the top channel and normalized by the day 0 counts. Data are represented as boxplots and analyzed with an unpaired t-test; *$p<0.05$.

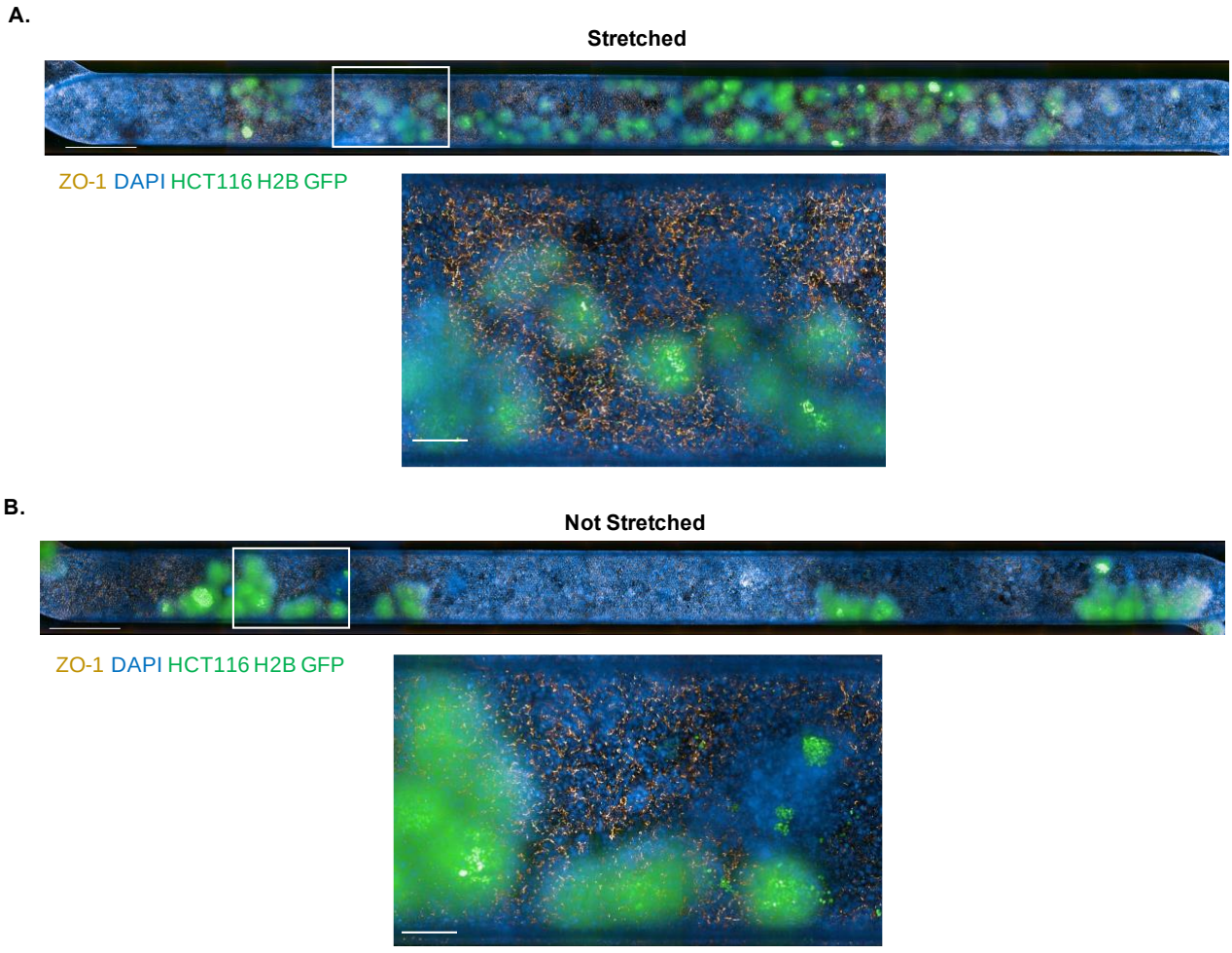

Figure S6. Peristalsis does not noticeably change tight junction formation in HCT116-CRC-on-Chips, Related to Figure 5. A. Tiled maximum projection (60 µm Z-height) and zoomed-in (white box) confocal fluorescent images of the epithelial channel of the HCT116-CRC-on-Chip on day 6 in the presence of cyclic peristalsis-like motions. Chips were stained for tight junction protein ZO-1 (gold). HCT116 tumor cells are labeled with H2B GFP (green) and cell nuclei are labeled with DAPI (blue). Scale bar represents 1 mm on the tiled image and 200 µm on the zoomed-in image. **B.** Tiled maximum projection (60 µm Z-height) and zoomed-in (white box) confocal fluorescent images of the epithelial channel of the HCT116-CRC-on-Chip on day 6 in the absence of cyclic peristalsis-like motions. Chips were stained for tight junction protein ZO-1 (gold). Images are not representative of HCT116 cluster number or distribution throughout the channel, as clusters may be lost during the fixation and immunofluorescence process, particularly in the not stretched conditions. HCT116 tumor cells are labeled with H2B GFP (green) and cell nuclei are labeled with DAPI (blue). Scale bar represents 1 mm on the tiled image and 200 µm on the zoomed-in image.

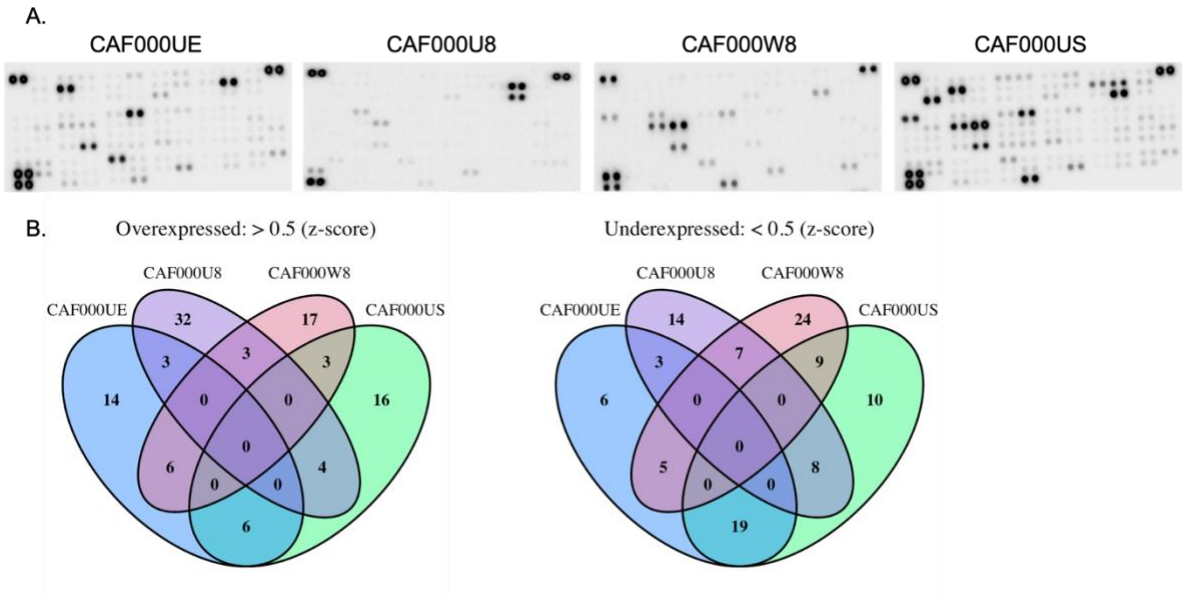

Figure S7. Patient-derived CAFs show heterogeneous cytokine profiles, Related to Figure 5 and Tables S8 and S9. (A) Raw images of cytokine array blots performed on conditioned media collected from patient-derived CAFs. **(B)** Cytokine and growth factor expression was evaluated via cytokine arrays. Z-scores were determined and the overlap of upregulated and downregulated cytokines (> or < 0.5 fold) across CAF lines is shown. Refer to Tables S8 and S9 for cytokine details. N=2 lots of CM for each CAF.

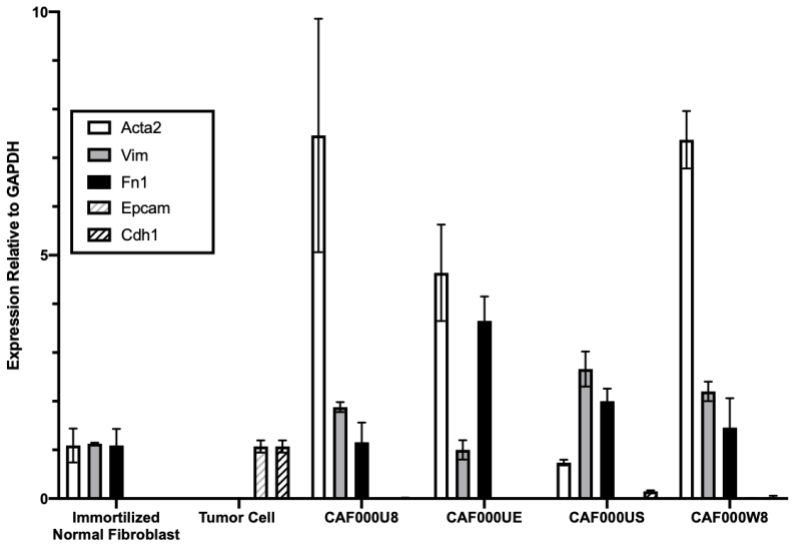

Figure S8. Validation of CAFs isolated from patient tissues, Related to Figure 5 and STAR Methods. qPCR analysis of CAF-associated markers: alpha smooth muscle actin (*Acta2*), fibronectin (*Fn1*), and vimentin (*Vim*) and epithelial markers: EpCam (*Epcam*) and E-Cadherin (*Cdh1*) was performed on primary CAF cells isolated from patients 000UE, 000U8, 000US, and 000W8, CRC tumor cells (HCT116), and an immortalized normal fibroblast cell line (CCD18Co) (N=3 replicates). Data are represented as mean ± SEM.